BIOCHEMISTRY
including biophysical chemistry & molecular biology

Article

pubs.acs.org/biochemistry

Differential Dynamics of Extracellular and Cytoplasmic Domains in Denatured States of Rhodopsin

Arpana Dutta,[†] Christian Altenbach,[‡] Sheryll Mangahas,[‡] Naveena Yanamala,[†] Eric Gardner,[†] Wayne L. Hubbell,[‡] and Judith Klein-Seetharaman*[,†,§]

[†]Department of Structural Biology, University of Pittsburgh School of Medicine, Pittsburgh, Pennsylvania 15260, United States

[‡]Jules Stein Eye Institute and Department of Chemistry & Biochemistry, University of California, Los Angeles, California 90095-7008, United States

[§]Division of Metabolic and Vascular Health, Medical School, University of Warwick, Coventry CV4 7AL, U.K.

ABSTRACT: Rhodopsin is a model system for understanding membrane protein folding. Recently, conditions that allow maximally denaturing rhodopsin without causing aggregation have been determined, opening the door to the first structural characterization of denatured states of rhodopsin by nuclear magnetic resonance (NMR) and electron paramagnetic resonance (EPR) spectroscopy. One-dimensional ^{1}H NMR spectra confirm a progressive increase in flexibility of resonances in rhodopsin with increasing denaturant concentrations. Two-dimensional ^{1}H−^{15}N HSQC spectra of [^{15}N]-α-lysine-labeled rhodopsin in which signals arise primarily from residues in the cytoplasmic (CP) domain and of [^{15}N]-α,ε-tryptophan-labeled rhodopsin in which signals arise only from transmembrane (TM) and extracellular (EC) residues indicate qualitatively that EC and CP domains may be differentially affected by denaturation. To obtain residue-specific information, particular residues in EC and CP domains were investigated by site-directed spin labeling. EPR spectra of the spin-labeled samples indicate that the EC residues retain more rigidity in the denatured states than the CP residues. These results support the notion of residual structure in denatured states of rhodopsin.

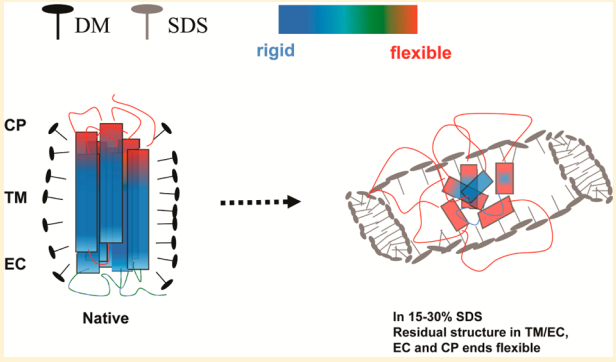

When proteins are subjected to increasingly denaturing conditions, they progressively lose secondary and tertiary structure. The resulting non-native states are ensembles of states because they are highly dynamic and can thus not be described as a single conformation. The presence of residual structure in such ensembles of denatured states is well-known for soluble proteins.[1−3] High-resolution structural characterization of denatured states of proteins is one way to obtain information about the propensity of interactions among residues in early stages of folding. Determining the motion of residues in denatured states is thus a direct measure of their involvement in interactions.[4,5] The extent to which residual structure is retained in the denatured states of membrane proteins and the nature of such residual structure are not known. Numerous membrane proteins have been reversibly unfolded and refolded but typically not to or from a fully random coil state (reviewed in ref 6): *in vitro* unfolding studies uniformly show the difficulty in denaturing membrane proteins; usually large regions of structure remain intact despite the presence of high denaturant concentrations.[7−12] In fact, bR[13] and CopA[14] are to date the only helical membrane proteins that have been almost fully unfolded. It is thermodynamically unlikely that membrane proteins will be completely unfolded inside the membrane environment *in vivo* or in the membrane mimetics used to study these proteins *in vitro*. Thus, for membrane proteins, residual structure may actually play an even more important role for folding than in soluble proteins. It is critical for our understanding of membrane protein folding mechanisms to characterize the molecular nature of denatured states that are an ensemble of states observed under given denaturing conditions. With an increasing denaturant concentration, a new ensemble of unfolded states that are all unfolded to a different extent compared to that of the ensemble at the previously used concentration is formed. Of particular interest are those ensembles of denatured states found under the most denaturing conditions used. For membrane proteins, no in-depth characterization of the structure and dynamics in these most denatured states, where the majority of secondary structure is unfolded, exists. This is largely due to the difficulties in working with membrane proteins, which are prone to aggregation, especially in the presence of denaturants where the membrane-spanning regions are no longer in their native environment.

A recent screen of denaturing conditions simultaneously maximizing the extent of denaturation while preventing aggregation have identified 30% SDS or 3% SDS with 8 M

Received: July 12, 2014
Revised: September 30, 2014
Published: September 30, 2014

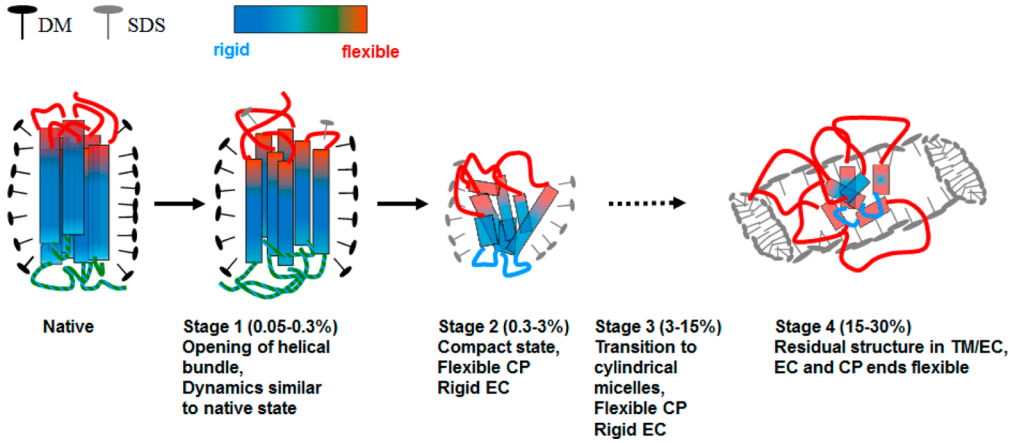

Figure 1. Model representing global and domain-specific changes in denatured states. TM regions of native rhodopsin are shown as cylinders with the colors corresponding to different degrees of flexibility as shown in the color bar. Stage 1 represents changes occurring at low SDS concentrations (0.05−0.3%) where opening of the helical bundle occurs. This is followed by stage 2, where with an increase to a SDS concentration of 3%, a compact state is formed with rigid regions in EC and TM domains. Beyond 3% SDS, a transition to cylindrical micelles occurs followed by formation of compact states in cylindrical micelles in 30% SDS in stage 4, where residual structure is formed in the TM and EC region.

urea (3S8U) as suitable conditions for studying largely denatured states of rhodopsin.[15] However, the molecular nature of these unfolded states, and whether there are differences between them, was not known and is the subject of this work. Our previous study showed that addition of increasing amounts of SDS to rhodopsin in dodecyl maltoside (DM) micelles denatured the protein in four stages (Figure 1). These stages were identified by circular dichroism (CD) spectroscopy.[15] Mean residue ellipticity (MRE) at 222 nm indicative of α-helix content decreased abruptly at a SDS concentration of 0.05−0.3% (stage 1) and then remained constant until 3% (stage 2). In this concentration range, SDS forms spherical micelles.[16] With further increases in SDS concentration, rhodopsin lost secondary structure in stage 3, where the spherical micelles undergo a transition to cylindrical micelles,[16] and the latter predominate in stage 4, where maximal denaturation is observed at the highest possible SDS concentration of 30%. Approximation of helix content from the CD spectra suggested that at this concentration 45% of the native helix content is lost. A similar loss of helix content was reported for 3S8U.

The changes in global structure with increasing concentrations of SDS have also been characterized by several complementary time-resolved and steady state spectroscopic measurements.[17] They confirmed the progression of denaturation in four stages and further identified that denatured states in SDS spheres and cylinders show a relatively greater burial of cysteine and tryptophan residues and are more compact than the states observed in mixed micellar structures. Protein structural changes at the membrane/water interface region were most prominent at very low SDS concentrations but reached transient stability in the compact conformations in SDS spheres. These studies therefore supported the hypothesis that a compact intermediate is formed in the denatured states. Compact intermediates have been suggested by the long-range interaction theory of folding of membrane proteins that proposes that interactions involving loops and transmembrane (TM) helices form during early folding stages.[18] The model was based on computational simulation of thermal denaturation of rhodopsin that had predicted the existence of a folding core involving loops and TM helices near the extracellular (EC) surface of rhodopsin.[19] The residues implicated to be part of the folding core are highlighted by green circles in the secondary structure representation shown in Figure 2 and include EC loops E-I and E-II, residues in the N-terminal tail, and some portions of TM helices 3−5 toward their EC sides.

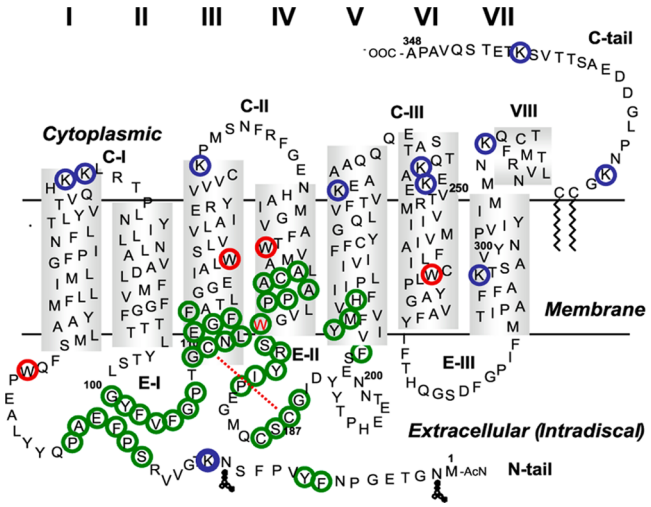

Figure 2. Secondary structure representation of rhodopsin showing predicted folding core residues[19] in green circles, tryptophans in red circles, and lysines in blue circle.

Here, we present the first attempt to characterize the structure and dynamics of denatured states of membrane proteins, using rhodopsin as a model over a range of SDS concentrations up to 30%, and in 3S8U. We adopted a combined NMR and EPR spectroscopic approach. NMR spectroscopy has seen significant advances recently in studies of α-helical membrane proteins.[20−23] Particularly for rhodopsin, extensive studies incorporating ^{15}N, ^{15}N/^{13}C, and ^{19}F labels have shown the applicability of NMR to this system in the folded state.[24−30] Here, we use NMR spectroscopy of [^{15}N]-α-lysine- and [^{15}N]-α,ε-tryptophan-labeled rhodopsin to obtain a characterization of denatured states that is more in-depth than what is possible with global biophysical approaches such as CD and fluorescence spectroscopy. Because the assignment of signals is still problematic, we also obtained residue-specific

dx.doi.org/10.1021/bi401557e | Biochemistry 2014, 53, 7160−7169

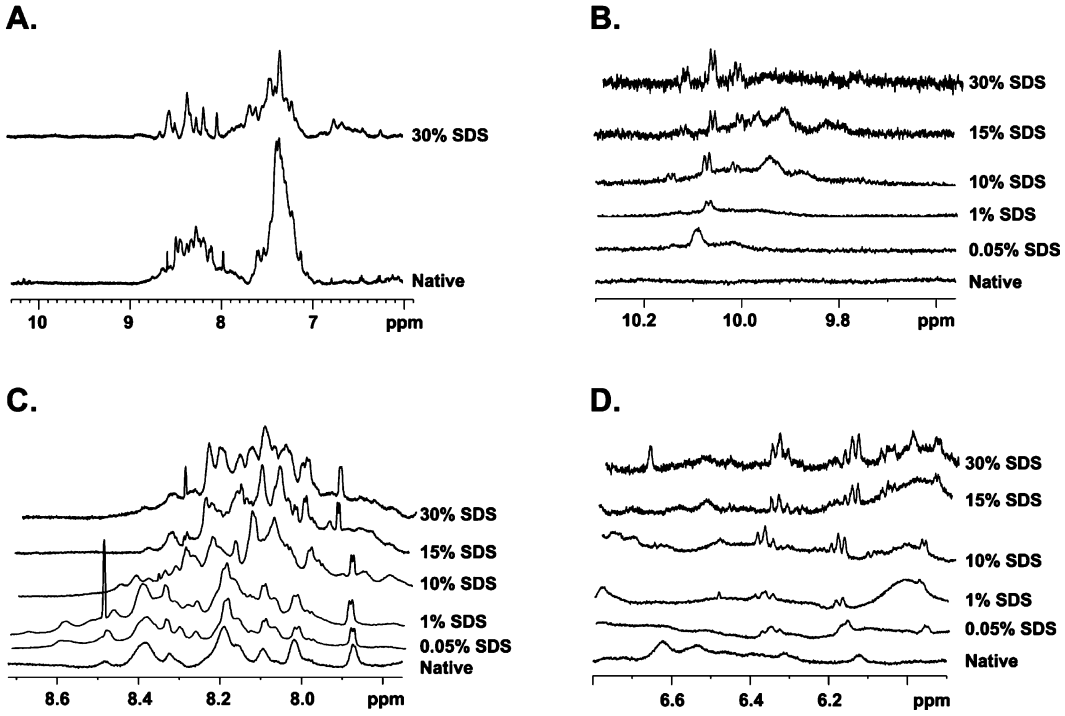

Figure 3. One-dimensional ^{1}H spectra of native and denatured rhodopsin. Overlay of native and 30% SDS-denatured rhodopsin showing the region from 6 to 10.3 ppm. (A) Overlays of native rhodopsin and 0.05, 1, 10, 15, and 30% SDS-denatured rhodopsin in the region around 10 (B), 8 (C), and 6 ppm (D).

information by using site-directed spin labeling with the nitroxide side chain. This method has been very well established for studying structure and structural changes in the cytoplasmic (CP) domain of rhodopsin in its dark- and light-activated states by specifically mutating residues of interest to cysteines and labeling them with spin labels.[31−38] Here, we used site-directed spin labeling to follow residue-specific conformational changes upon denaturation of rhodopsin using EPR spectroscopy. The NMR and EPR results locate the positions of residual structure to a cluster of residues that as a minimum contains V204 and I205 and likely extends to the full predicted folding core region (Figure 2, green) involving the EC ends of helices III−V and possibly two or three turns toward the membrane interior involving tryptophan residues (Figure 2, red), residues in E-I, E-II, and the N-terminal tail. This residual structure would explain the compactness as observed by global characterization of denatured states of rhodopsin.[17] Residual structure was observed under both maximally denaturing conditions, 30% SDS and 3S8U, but the structure appeared to be overall more restricted in 3S8U than in 30% SDS, indicating that 30% is a more drastically denaturing condition. However, the difference between CP and EC residues was clearly visible under both conditions.

MATERIALS AND METHODS

SDS (electrophoresis grade) was purchased from Bio-Rad (Hercules, CA) and dodecyl maltoside (DM) from Anatrace (Maumee, OH). Deuterated SDS and urea, deuterium oxide, [^{15}N]-α-lysine, and [^{15}N]-α,ε-tryptophan were purchased from Cambridge Isotope Laboratories (Cambridge, MA), and the methanethiosulfonate spin label (MTSL) was from Toronto Research Chemicals (Toronto, ON). Rhodopsin for NMR studies was purified from a tetracycline inducible HEK 293S cell line stably transfected with the wild-type opsin gene, as described previously.[26] All samples were purified in 10 mM sodium phosphate buffer containing 0.05% DM. Rhodopsin mutants for EPR studies (N151C, I154C, M155C, T108C, V204C, and I205C) were obtained by site-directed mutagenesis according to the established Stratagene protocol. Mutants were expressed by DEAE-Dextran transient transfection of COS-1 cells and harvested after 60 h. Spin labeling to introduce the nitroxide side chain designated R1 and purification of each mutant were conducted on an immunoaffinity column as described previously.[39]

NMR Spectroscopy. All NMR experiments were conducted in a Bruker 900 MHz spectrometer at 37 °C. The [^{15}N]-α-lysine-labeled rhodopsin at 50 μM in 20 mM sodium phosphate buffer, 10% D_2O, and 0.5% DM and [^{15}N]-α,ε-tryptophan-labeled rhodopsin at 0.12 mM in the same buffer but with 1.2% DM were used to record NMR spectra. A 0.15 mM [^{15}N]-α,ε-tryptophan-labeled sample was used to record the native two-dimensional (2D) HSQC spectrum. All one-dimensional (1D) ^{1}H spectra were referenced to DSS (4,4-dimethyl-4-silapentane-1-sulfonic acid). 1D spectra were recorded using the pulse program p3919gp.[40] 2D spectra were not referenced to any external standard. The numbers of scans for all denatured 2D HSQC spectra of [^{15}N]-α-lysine-labeled rhodopsin were 256 and 80 in the ^{15}N and ^{1}H dimensions, respectively, except for 3S8U at pH 2 for the denatured sample (2000 and 48, respectively); 128 × 48 scans were used to record the native state spectrum for this sample. The numbers of scans for all denatured 2D HSQC spectra of [^{15}N]-α,ε-tryptophan-labeled rhodopsin were 2000 and 42, respectively, except for the native state (1000 and 72, respectively).

EPR Spectroscopy. EPR spectra were recorded at room temperature on a Bruker ELEXSYS 580 instrument using the High Sensitivity Resonator (Bruker). Each spectrum is the

dx.doi.org/10.1021/bi401557e | Biochemistry 2014, 53, 7160−7169

average of 25 scans of 30 s each over a range of 100 G. Samples (6 μL) at protein concentrations of 50−100 μM were placed in 0.6 (inside diameter) × 0.84 (outside diameter) borosilicate capillary tubes. All samples were in 5 mM MES [2-(morpholino)ethanesulfonic acid] buffer with DM concentrations varying from 3 to 5%.

RESULTS

Changes in Overall Protein Dynamics. Because identification of residual structure in denatured proteins relies largely on finding restriction in conformational space, measurement of protein dynamics is the most direct approach.[4] We have therefore studied qualitatively the global motions experienced by rhodopsin residues under denaturing conditions by measuring 1D ^{1}H NMR spectra in the presence and absence of different denaturants. Figure 3A shows a comparison between the 1D spectrum of native and 30% SDS-denatured rhodopsin, which is its maximally denatured state.[15] The native state spectrum shows broad and overlapping peaks caused by the presence of 348 amino acids that cannot be resolved on a 1D ^{1}H spectrum. Further, it was observed previously that backbone amides of tryptophans and lysines show more than the expected number of signals with varying intensities in the NMR spectrum of [^{15}N]-α-lysine-labeled and [^{15}N]-α,ε-tryptophan-labeled rhodopsin.[26,27] These observations indicated that there are conformational fluctuations on a microsecond to millisecond time scale leading to signal broadening. In the presence of 30% SDS, the number of the resolved proton peaks increases, supporting the hypothesis that an increase in the level of motion from the microsecond to millisecond time scale to nanosecond time scales of motion in unfolded regions of the protein is taking place. Although more quantitative relaxation measurements are needed to prove this hypothesis, this shift to rapid motion (nanoseconds or faster) of unfolded regions in a protein will be henceforth termed qualitatively an increase in flexibility upon denaturation. Panels B−D of Figure 3 show the aromatic side chain region [around 10 ppm (Figure 3B)], the backbone [around 8 ppm (Figure 3C)], and the further upfield regions, where side chains and backbone protons of some amino acids appear [around 6 ppm (Figure 3D)]. In all regions, peaks that are not observed in native rhodopsin appear upon addition of SDS, indicating their enhanced flexibility. The changes in ^{1}H NMR spectra fit well with our previous observation of four stages based on circular dichroism spectroscopy (Figure 1). Stage 1 (represented by the 0.05% spectrum) is characterized by an appearance very similar to that of the native state, which remains similar even in stage 2 (represented by the 1% spectrum). The similarity is particularly apparent in Figure 3C. The next stages, stages 3 and 4, differ dramatically from stages 1 and 2 and are again similar to each other. This indicates that the NMR spectra are strongly affected by the shape of the micelles, spherical in stages 1 and 2 and cylindrical in stages 3 and 4.

Identification of Flexible and Rigid Regions in SDS-Denatured States. To determine dynamics more specifically, we compared the motions of denatured regions of rhodopsin carrying isotope labels that preferentially label TM and EC versus CP residues. Tryptophans, labeled with ^{15}N at its backbone and side chain nitrogens, and lysines, labeled with ^{15}N at its backbone nitrogen, were used as reporters. This is because with the exception of Lys296, the TM attachment site for retinal, and one lysine near the N-terminus (Lys16), all other lysine residues are located in the CP domain (Figure 2, blue circles). In contrast, tryptophans are observed in only the TM and EC domains (Figure 2, red circles). This allows us to obtain higher-resolution structural information than with ^{1}H spectra alone. The folding core is predicted to be located at the interface between TM and EC domains (Figure 2, green circles).[19] Thus, we expect tryptophan residues to be more rigid under denaturing conditions than lysine residues.

An overlay of 2D heteronuclear single-quantum correlation (HSQC) spectra of 1% SDS-denatured (stage 2) and 30% SDS-denatured (stage 4) [^{15}N]-α,ε-tryptophan-labeled rhodopsin is shown in panel 1 of Figure 4A. The corresponding spectrum of native rhodopsin is shown in panel 2 and is identical to that reported previously.[27] The native spectrum is characterized by a number of tryptophan backbone peaks larger than the number of tryptophans in the structure due to conformational heterogeneity, while the expected five side chain peaks are observed for the five tryptophan residues in rhodopsin.[27] In panel 1 of Figure 4A, at 1% SDS (green), fewer backbone peaks and clustering of the side chain peaks are observed compared to case for the native state, supporting the significant overall reduction of secondary and tertiary structure revealed by CD[15]

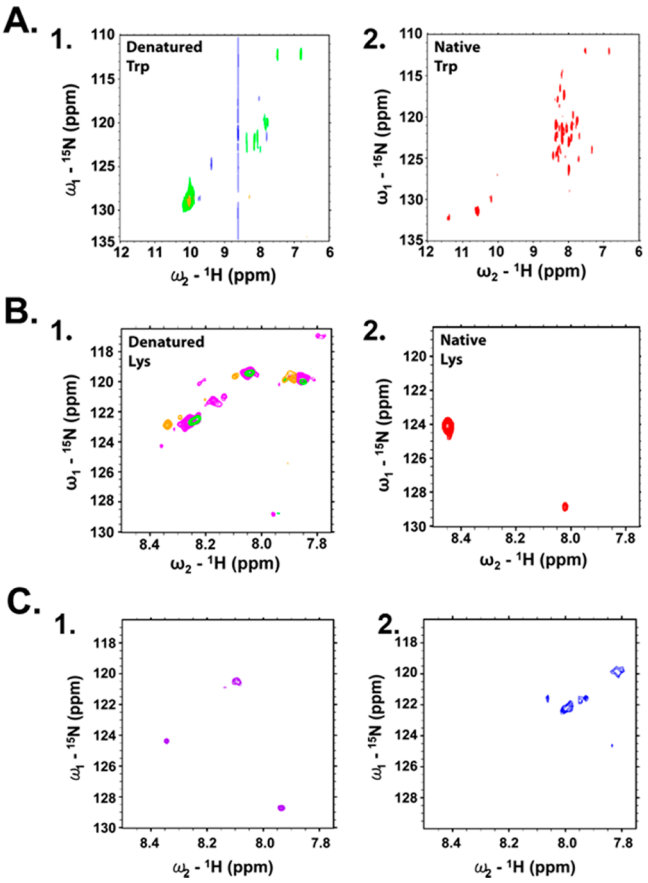

Figure 4. 2D HSQC spectra of native and denatured isotope-labeled rhodopsin. (A) Overlay of 2D HSQC spectra of [^{15}N]-α,ε-tryptophan-labeled rhodopsin: (1) denatured with 1% SDS (green), 30% SDS (orange), and 3S8U (blue) and (2) 2D HSQC spectrum of native rhodopsin. (B) Overlay of 2D HSQC spectra of [^{15}N]-α-lysine-labeled rhodopsin: (1) denatured with 1% SDS (green), 10% SDS (magenta), and 30% SDS (orange) and (2) 2D HSQC spectrum of native rhodopsin. (C) Overlay of 2D HSQC spectra of denatured [^{15}N]-α-lysine-labeled rhodopsin: (1) denatured with 0.05% SDS and (2) denatured with 3S8U at pH 2.

dx.doi.org/10.1021/bi401557e | Biochemistry 2014, 53, 7160−7169

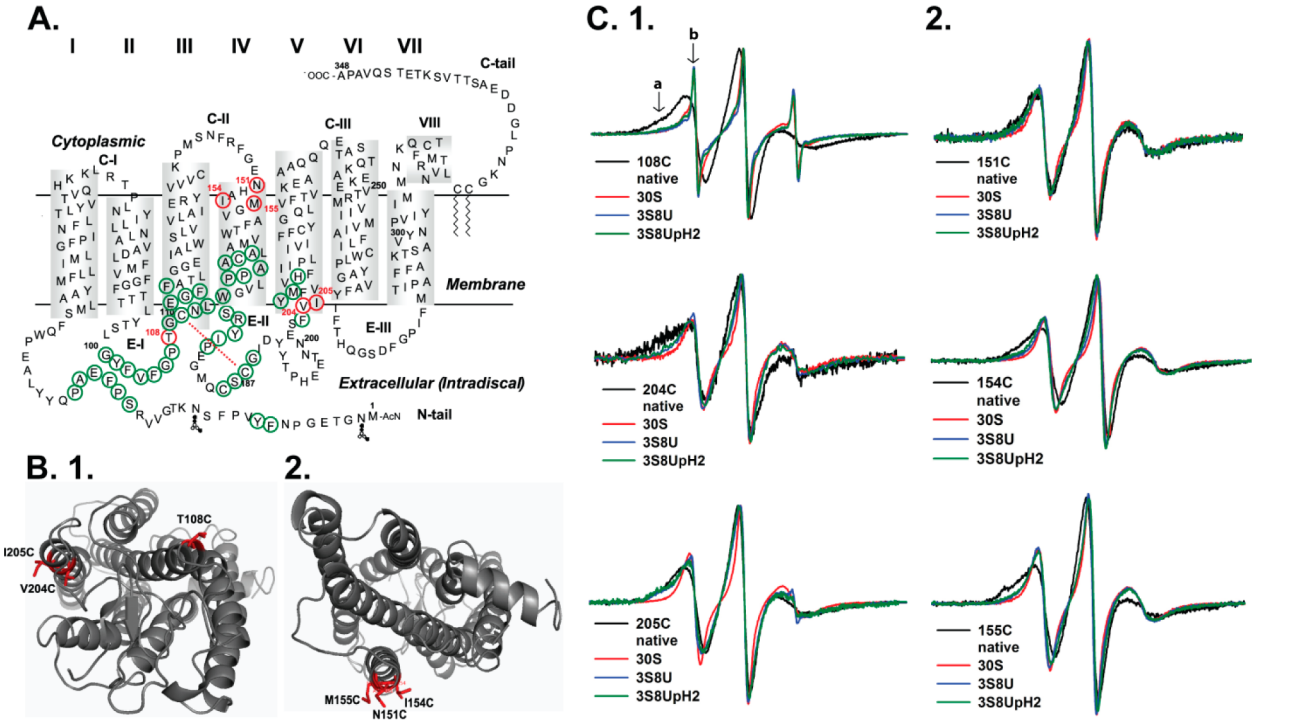

Figure 5. Continuous wave EPR (CW-EPR) spectra of native and denatured rhodopsin studied by EPR. (A) Secondary structure representation of rhodopsin showing predicted folding core residues in green circles and the residues studied by EPR in red circles. (B) Panel 1 shows the three-dimensional (3D) structure of rhodopsin viewed from the EC face with the EC residues studied by EPR colored red. Panel 2 shows the 3D structure of rhodopsin viewed from the CP face with the CP residues studied by EPR colored red. (C) Panel 1 shows an overlay of CW-EPR spectra for EC sites T108R1, V204R1, and I205R1 in the native state and treated with 30% SDS, 3S8U, and 3S8U at pH 2. Arrows marked a and b denote regions on the EPR spectra that represent relatively immobile and mobile components, respectively. Panel 2 shows an overlay of CW-EPR spectra for CP sites N151R1, I154R1, and M155R1 in the native state and treated with 30% SDS, 3S8U, and 3S8U at pH 2.

and fluorescence[17] spectroscopies. At 30% SDS (orange), which maximally unfolds rhodopsin, decreased background signal intensities were observed compared to that observed in the presence of 1% SDS (green). The side chain peaks remain clustered at a similar position (~10 ppm) but with intensities significantly lower than that at 1% SDS, suggesting that a residual structure containing tryptophan residues is retained even at this high SDS concentration.

In contrast to tryptophan residues, which probe the predicted folding core region extended by one or two turns of a helix into the transmembrane domain, lysine residues are located mostly away from the predicted folding core. In panel 1 of Figure 4B, an overlay of 2D HSQC spectra of 1, 10, and 30% SDS-denatured states is shown in comparison with the native spectrum (Figure 4B, panel 2). There are 11 lysines in rhodopsin, but the most intense peak originates from Lys339 in the C-terminal tail; other signals had intensities that were <10% of that of Lys339.[26] Because of the low protein concentration of 50 μM used here, we observe only the Lys339 resonance. Comparing the HSQC spectra of the SDS-titrated protein with the spectrum of the native state, we see that the most intense peak observed in the native protein does not exist in SDS-treated samples but other peaks begin to appear. The intensity and number of backbone peaks increase with an increase in SDS concentration from 0.05% (Figure 4C, panel 1) to 1% (green) and finally to 10% (magenta), indicating an increase in the flexibility of lysines with an increase in the level of unfolding. At 30% SDS (orange), peak intensities decrease compared to those at 10% SDS but appear to be similar to those observed in the 1% SDS-denatured state except for the peaks around 120 and 7.9 ppm in ^{15}N and ^{1}H dimensions, respectively. These signals have a greater peak intensity in the 30% SDS-denatured state, indicating that in contrast to tryptophan residues, lysine residues are fully flexible under these conditions.

Mobility of Residues in the Predicted Folding Core (EC loops) in SDS. Following the indication from NMR spectroscopy that there is differential mobility upon denaturation upon comparison of CP versus TM and EC regions in rhodopsin, we collected residue-specific information about the mobility of three residues within the predicted folding core in the EC domain, T108R1, V204R1, and I205R1 (colored red in Figure 5A and B1). Continuous wave EPR (CW-EPR) spectra of these mutants in the native and denatured states were recorded. Because the shape of the spectrum is biased toward the most mobile component, they were normalized for equal height of the central peak to allow qualitative comparison of the immobile component. Mobile and immobile components of a CW-EPR spectrum as described in ref 42 are indicated by arrows a and b, respectively, in panel 1 of Figure 5C. The spectrum of T108R1, V204R1, and I205R1 in the native state shows two components, each corresponding to a different degree of mobility (Figure 5C, panel 1). Upon addition of SDS at increasing concentrations, a gradual decrease in the immobile component was seen (Figures 6 and 7), which is indicative of a direct relationship between higher residue mobility and an increasing level of denaturation. While samples in 0.05% SDS (Figure 6, orange lines) display a spectrum similar to the native one, suggesting that under these conditions the helical bundle is opened but the dynamics are similar to those of the native state,

dx.doi.org/10.1021/bi401557e | Biochemistry 2014, 53, 7160−7169

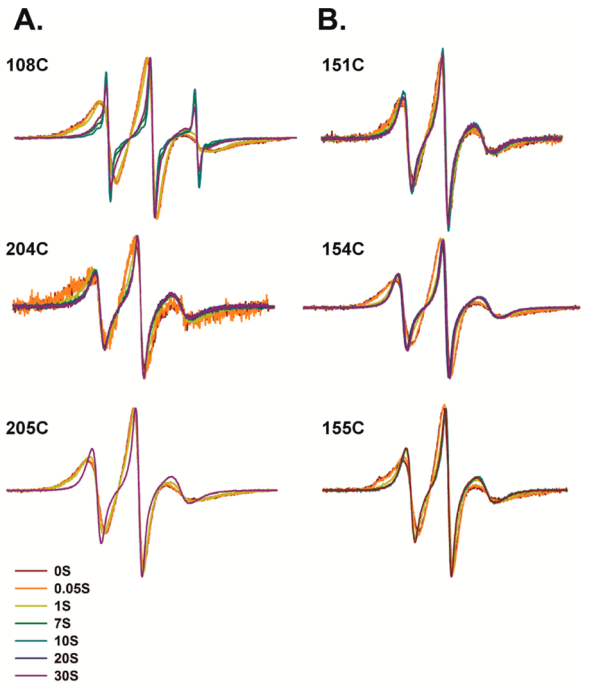

Figure 6. CW-EPR spectra of native and denatured states of EC and CP mutants studied by EPR. (A) Overlay of CW-EPR spectra of T108R1, V204R1, and I205R1 in the native state and treated with different SDS concentrations. (B) Overlay of CW-EPR spectra for N151R1, I154R1, and M155R2 in the native state and treated with different SDS concentrations.

a further small change is observed in 1% SDS (Figure 6, olive line), with more dramatic changes at the higher concentrations (Figure 6, from green to turquoise to blue to purple).

Mobility of Residues Away from the Predicted Folding Core (CP loops) in SDS. To compare the motions of folding core residues with that of residues away from the core, CW-EPR spectra of CP domain mutants, N151R1, I154R1, and M155R1 (colored red in the CP domain in Figure 5A,B2), in the native and denatured states were recorded. Comparing the native state spectra of N151R1, I154R1, and M155R1 in panel 2 of Figure 5C, we found the latter two mutants have an immobile component more dominant than that of N151R1. This component only slightly decreases with an increase in SDS concentration for N151R1 as seen in Figure 6B because it is already mobile in the native state. However, for the I154R1 mutant, the immobile component disappears from 1% SDS onward, whereas for the M155R1 mutant, a greater amount of immobile component is retained at 1% SDS, which completely disappears only at 10% SDS (Figure 6B). For all CP mutants at 30% SDS, there is no immobile component. This is in contrast with the results for the EC residues in which an immobile component was still retained in 1% SDS for all the residues tested and up to 7% for T108R1 and V204R1.

Dependence of the Mobility of EC and CP Residues on SDS Concentration. We also investigated if there are differences in the concentration of SDS required to mobilize residues fully when comparing EC and CP residues. Residues were compared pairwise on the basis of their relative positioning with respect to the helical bundle.

Figure 7 shows a comparison of CW-EPR spectra for pairs of residues at each denaturant concentration. Figure 7A shows the comparison of N151R1 (CP) and T108R1 (EC), residues located at the membrane interface, at the end of their helices and with side chains facing the aqueous environment. T108R1 appears to be slightly more immobile than N151R1 in the native state, which could be due to differences in backbone dynamics or the surrounding environment. At 1% SDS, this difference increases and T108R1 shows an immobile component greater than that of N151R1. However, from 7% SDS onward, T108R1 becomes very mobile. Spectra for 7 and 10% SDS-denatured states for T108R1 were obtained after 5 h because this was the amount of time needed for it to equilibrate, and no time dependent changes were observed

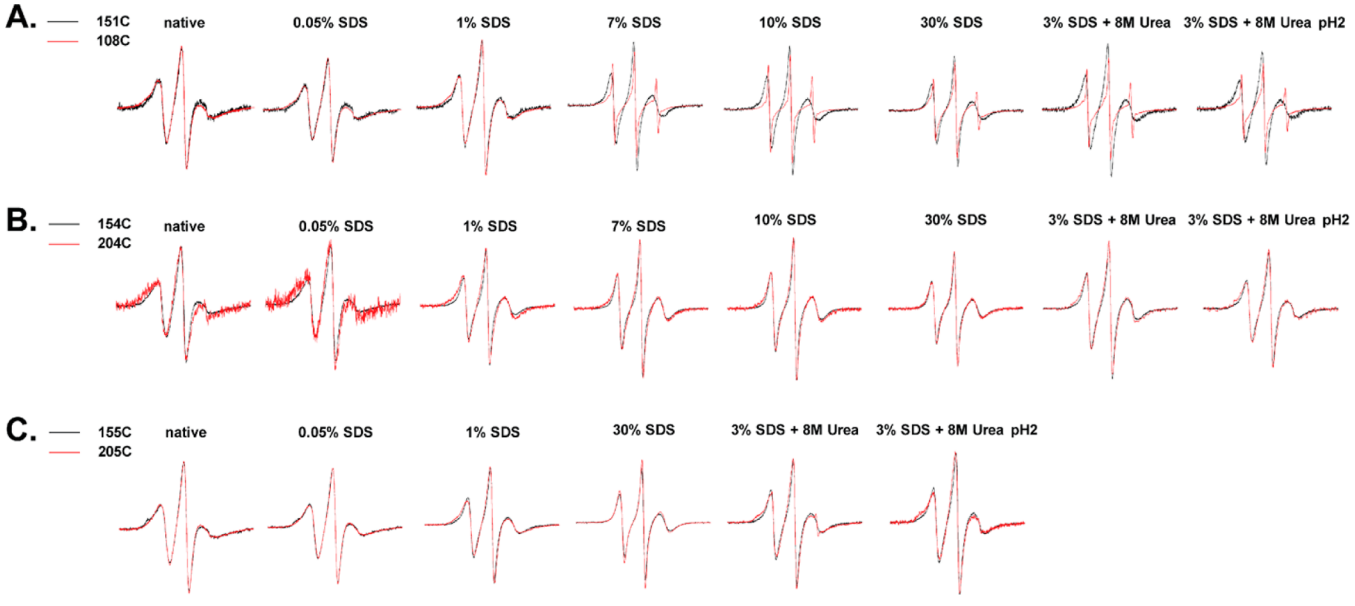

Figure 7. Comparison of CW-EPR spectra of native and denatured EC and CP residues. Overlays of EPR spectra of (A) T108R1 and N151R1, (B) V204R1 and I154R1, and (C) I205R1 and M155R1 in which each mutant is treated with different concentrations of SDS and with 3S8U and 3S8U at pH 2.

dx.doi.org/10.1021/bi401557e | *Biochemistry* 2014, 53, 7160−7169

for N151R1 at any SDS concentration or for that matter for any other mutant under any denaturing condition.

Figure 7B shows the comparison between I154R1 (CP) and V204R1 (EC). Both these residues are at the same membrane depth and at the same turn of the helix, but the side chain of I154R1 is slightly more exposed than that of V204R1. As we saw for the T108R1/N151R1 pair, the EC residue, V204R1, is more immobile than the corresponding CP residue, I154R1, in the native state. However, unlike T108R1 (EC), which becomes flexible from 7% SDS onward, immobility in V204R1 (EC) is retained more than in I154R1 up to 20% SDS. At 30% SDS, V204R1 is still slightly more immobile than I154R1. These results indicate that the EC residue, V204R1, shows rigidity in the denatured states greater than that of the corresponding CP residue.

Figure 7C shows the comparison between M155R1 (CP) and I205R1 (EC). Both these residues are equivalently placed with regard to membrane depth and position in the helix. In the native state, M155R1 has a slight immobile component compared to I205R1 in the native state. With a SDS concentration increasing to 0.05 and 1%, I205R1 becomes more immobile than M155R1, with both showing a similar spectrum at 30% SDS.

Comparison of Residual Structure under 3S8U Denaturing Conditions. Besides 30% SDS, our previous screen had identified 8 M urea as well as 3S8U as maximally denaturing conditions with decreases in mean residue ellipticity at 222 nm of 40−55%.[15] While 8 M urea also results in aggregation, 3S8U does not, allowing us to characterize this highly denatured state via NMR and EPR. An overlay of 2D heteronuclear single-quantum correlation (HSQC) spectra of 3S8U-denatured [^{15}N]-α,ε-tryptophan-labeled rhodopsin with the 1 and 30% SDS conditions is shown in panel 1 of Figure 4A. To avoid the urea background signal in the amide region of the spectrum, the pH was lowered to 2. According to CD, the denaturing efficiency of 3S8U at pH 2 is lower than that of 3S8U at neutral pH (data not shown), estimated to decrease the molar ellipticity of rhodopsin by only ∼25% as compared to ∼45%. As shown in the overlay in panel 1 of Figure 4A (blue), the backbone signals in 3S8U at pH 2 are fewer in number and lower in intensity than that in native and 1% SDS but are greater than that at 30% SDS. The side chain peaks appear to be less clustered than those in the spectra recorded in the native state and in the presence of 30% SDS, indicating that a different denatured state is formed in 3S8U at pH 2 than in 30% SDS. The differences observed are in line with the intermediate denaturing capacity of this condition suggested by CD. As in the study of tryptophans, we recorded an HSQC spectrum of [^{15}N]-α,ε-lysine-labeled rhodopsin in the presence of 3S8U at pH 2 as shown in panel 2 of Figure 4C. Unlike the case with tryptophans, here larger numbers of scans (see Materials and Methods) were needed to obtain a suitable signal-to-noise ratio compared to the SDS-titrated samples, indicating formation of a different denatured state with slower dynamics compared to those of the SDS denatured samples.

We also recorded EPR spectra of all mutants under 3S8U conditions. Spectra of EC mutants T108R1, V204R1, and I205R1 denatured with 3S8U and 3S8U at pH 2 are overlaid with that of the native and 30% SDS-denatured proteins to compare the maximally denatured states in panel 1 of Figure 5C. It is evident that states denatured with 3S8U and 3S8U at pH 2 retain a more immobile component than the 30% SDS-denatured state for all EC mutants. This difference is most clearly evident for I205R1. In panel 2 of Figure 5C, the spectra of CP mutants denatured with 3S8U and 3S8U at pH 2 are overlaid with those of native and 30% SDS-denatured protein to compare the maximally denatured states. Similar to what we observed for EC residues, the states denatured with 3S8U and 3S8U at pH 2 retain more immobile components than the 30% SDS-denatured state for all CP mutants (Figures 5−7). The immobility of I205R1 is pronounced to a great extent when the mixture of SDS and urea is used as a denaturant. Here again, it is seen that the EC residue is in a more structured environment than the corresponding CP residue. These results support the conclusion from NMR spectroscopy that a less dynamic state is formed in 3S8U than in 30% SDS, suggesting that the molecular nature of denatured states of rhodopsin is dependent on the chemical nature of the denaturants used.

DISCUSSION

Our recent optimization of denaturing conditions that lead to the greatest possible unfolding without aggregation of rhodopsin has opened the door to in-depth characterization of largely unfolded states of rhodopsin.[15] The extent of denaturation was judged on the basis of CD, which is a global characterization method from which we concluded that the maximally denatured states that did not also result in aggregation, 30% SDS and 3S8U, had lost some 50% of their helical content. Because CD does not allow conclusions about the location of this residual structure to be reached, we further studied the SDS-denatured states with several other biophysical approaches.[17] Absorption spectroscopy relies on the retinal located in the TM domain facing the EC side; steady state and time-resolved fluorescence spectroscopies are based on tryptophan residues predominantly located in the TM domain, and cysteine accessibility is based on the locations of cysteines, two of which reside in the CP domain and are accessible in the native state. Furthermore, we measured the size of intermediates using light scattering and fluorescence depolarization. This initial characterization provided evidence of a compact intermediate implying the possibility of "folding core"-like interactions responsible for the decrease in the overall size of the denatured states.[17] The qualitative locations of cysteine and tryptophan residues indicated that the earliest disruption of structure is located at the CP surface. To test this hypothesis, we attached a fluorescein reporter to Cys316 in the CP domain and showed that its tertiary interactions are lost already at the lowest SDS concentration of 005% studied, with biphasic behavior following the changes from stage 1 to stage 2.[17]

To quantitatively test the hypothesis from our previous computational[18,41] and experimental[17] studies that CP and EC domains are differentially affected by denaturation, here we employed biophysical techniques that allow simultaneous probing of EC and CP domains and/or residues with the same approach. We report on structural features of specific residues to isolate the position of residual structure in the compact states identified in our previous work by using NMR and EPR, as both techniques rely on reporter chemical groups that can be localized to EC and CP domains for the NMR approach used and specific residues within these domains for the EPR approach used. The NMR approach in principle also provides residue-specific information, but because of the challenges in assignment, interpretation currently remains at the domain level. To the best of our knowledge, this is the first time that residue-specific methods are being used in structural characterization of unfolded states of polytopic integral helical

membrane proteins. Collectively, the two approaches support the conclusion that there is a difference in the motions of EC and TM domains as compared to the CP domain in denatured states of rhodopsin. This finding experimentally supports the long-range theory for membrane protein folding that was based on theoretical considerations.[18,43] One cysteine investigated here does not follow this general trend between CP and EC residues, namely T108. This residue appears to be more mobile than any other residue in the denatured state, and it is an EC residue. However, this residue was not predicted to be part of the folding core (Figure 1). The glycine amino acid at position 109 and the proline amino acid at position 107 are immediate neighbors of T108, which contributes to the lack of contacts made with the structurally rigid cluster nearby. This result emphasizes the power of the site-directed approach afforded by EPR spectroscopy in validating details of the predictions and lends strong support to the validity of the location of the predicted folding core.

In our previous studies of optimization of denaturing conditions of rhodopsin, we have observed four stages in unfolding of TM helices (as recorded by CD spectroscopy) when SDS is added as a denaturant,[15] as depicted in Figure 1. These stages correlate with SDS micellar structural changes whereby in stage 1, mixed SDS/DM micelles are formed followed by formation of SDS spherical micelles in stage 2 that show a transition in stage 3 to form cylindrical micelles in stage 4.[44] Characterization of the global tertiary structure of denatured states also corroborates these stages.[15] Via combination of earlier studies with the one reported here, a model in which micellar structural changes and structural changes of denatured rhodopsin correlate with dynamics in different SDS concentration ranges emerges. We have updated Figure 1 to include reference to the dynamic information from this paper. At low SDS concentrations (0.05−0.3%), where we saw initial opening of the helical bundle,[17] we now know that the motions of the EC and CP domains are similar to those of the native state. At concentrations of SDS between 0.3 and 3%, where earlier studies had supported formation of a compact state,[17] current residue-specific studies show this compactness to be in the EC region. The rigidity of this domain still remains in stage 3 (3−15% SDS), where further unfolding along with a transition of spherical SDS micelles to cylindrical ones occurs. Finally, in maximally unfolded states, the data reported here support the notion that there is a compact intermediate, as suggested previously.[17] In these unfolded states, the CP and EC ends have become flexible but residual structure remains in the TM and EC regions, specifically in a core of structural stability that resists unfolding.

Because the location of the folding core correlates with residues implicated in misfolding of rhodopsin that have been studied extensively because of their mutation in patients affected by the degenerative disease of the retina, retinitis pigmentosa,[19] it is tempting to speculate that our experimental identification of this folding core may lead to a better understanding of misfolding of rhodopsin and its association with the disease. Indeed, we plan to conduct studies of the most frequent retinitis pigmentosa mutant P23H under denaturing conditions to test the hypothesis that the folding core may be disrupted in some way in this mutant. However, it is important to remind the reader that folding *in vivo* takes place with the membrane composed of complex lipid mixtures and cellular machinery assisting in folding present, so our *in vitro* studies have to be interpreted with this caveat in mind.

AUTHOR INFORMATION

Corresponding Author

*Division of Metabolic and Vascular Health, Warwick Medical School, Gibbet Hill, Rm. B037, University of Warwick, Coventry CV4 7AL, U.K. E-mail: j.klein-seetharaman@warwick.ac.uk. Phone: +44(0)2476573806.

Funding

This work was in part supported by National Science Foundation Grants CC044917 and 1144281, National Institutes of Health Grant 2R01LM007994-05, and EU Marie Curie Actions International Incoming Fellowship 626470 MPFP FP7-PEOPLE-2013-IIF. Support for W.L.H. was provided by NIH grants 5R01 EY05216, 2P30 EY0331, and the Jules Stein Professor endowment.

Notes

The authors declare no competing financial interest.

ABBREVIATIONS

CD, circular dichroism; CP, cytoplasmic; DM, dodecyl maltoside; EC, extracellular; HSQC, heteronuclear single-quantum correlation; TM, transmembrane; SDS, sodium dodecyl sulfate; 3S8U, 3% SDS with 8 M urea; R1, nitroxide side chain attached to cysteine.

REFERENCES

(1) Cho, J. H., Sato, S., Horng, J. C., Anil, B., and Raleigh, D. P. (2008) Electrostatic interactions in the denatured state ensemble: Their effect upon protein folding and protein stability. *Arch. Biochem. Biophys. 469*, 20−28.

(2) Daggett, V., and Fersht, A. R. (2003) Is there a unifying mechanism for protein folding? *Trends Biochem. Sci. 28*, 18−25.

(3) Shortle, D. (1996) The denatured state (the other half of the folding equation) and its role in protein stability. *FASEB J. 10*, 27−34.

(4) Klein-Seetharaman, J., Oikawa, M., Grimshaw, S. B., Wirmer, J., Duchardt, E., Ueda, T., Imoto, T., Smith, L. J., Dobson, C. M., and Schwalbe, H. (2002) Long-range interactions within a nonnative protein. *Science 295*, 1719−1722.

(5) Shortle, D., and Ackerman, M. S. (2001) Persistence of native-like topology in a denatured protein in 8 M urea. *Science 293*, 487−489.

(6) Tastan, O., Dutta, A., Booth, P., and Klein-Seetharaman, J. (2014) Retinal proteins as model systems for membrane protein folding. *Biochim. Biophys. Acta 1837*, 656−663.

(7) Barrera, F. N., Renart, M. L., Molina, M. L., Poveda, J. A., Encinar, J. A., Fernandez, A. M., Neira, J. L., and Gonzalez-Ros, J. M. (2005) Unfolding and refolding in vitro of a tetrameric, α-helical membrane protein: The prokaryotic potassium channel KcsA. *Biochemistry 44*, 14344−14352.

(8) Dockter, C., Volkov, A., Bauer, C., Polyhach, Y., Joly-Lopez, Z., Jeschke, G., and Paulsen, H. (2009) Refolding of the integral membrane protein light-harvesting complex II monitored by pulse EPR. *Proc. Natl. Acad. Sci. U.S.A. 106*, 18485−18490.

(9) Lau, F. W., and Bowie, J. U. (1997) A method for assessing the stability of a membrane protein. *Biochemistry 36*, 5884−5892.

(10) Miller, D., Charalambous, K., Rotem, D., Schuldiner, S., Curnow, P., and Booth, P. J. (2009) In vitro unfolding and refolding of the small multidrug transporter EmrE. *J. Mol. Biol. 393*, 815−832.

(11) Otzen, D. E. (2003) Folding of DsbB in mixed micelles: A kinetic analysis of the stability of a bacterial membrane protein. *J. Mol. Biol. 330*, 641−649.

(12) Plumley, F. G., and Schmidt, G. W. (1987) Reconstitution of chlorophyll a/b light-harvesting complexes: Xanthophyll-dependent assembly and energy transfer. *Proc. Natl. Acad. Sci. U.S.A. 84*, 146−150.

(13) Huang, K. S., Bayley, H., Liao, M. J., London, E., and Khorana, H. G. (1981) Refolding of an integral membrane protein.

Denaturation, renaturation, and reconstitution of intact bacteriorhodopsin and two proteolytic fragments. *J. Biol. Chem. 256*, 3802−3809.
(14) Roman, E. A., Arguello, J. M., and Gonzalez Flecha, F. L. (2010) Reversible unfolding of a thermophilic membrane protein in phospholipid/detergent mixed micelles. *J. Mol. Biol. 397*, 550−559.
(15) Dutta, A., Tirupula, K. C., Alexiev, U., and Klein-Seetharaman, J. (2010) Characterization of membrane protein non-native states. 1. Extent of unfolding and aggregation of rhodopsin in the presence of chemical denaturants. *Biochemistry 49*, 6317−6328.
(16) Nagarajan, R., Shah, K. M., and Hammond, S. (1982) Viscometric detection of sphere to cylinder transition and polydispersity in aqueous micellar solutions. *Colloids Surf. 4*, 147−162.
(17) Dutta, A., Kim, T. Y., Moeller, M., Wu, J., Alexiev, U., and Klein-Seetharaman, J. (2010) Characterization of membrane protein non-native states. 2. The SDS-unfolded states of rhodopsin. *Biochemistry 49*, 6329−6340.
(18) Klein-Seetharaman, J. (2005) Dual role of interactions between membranous and soluble portions of helical membrane receptors for folding and signaling. *Trends Pharmacol. Sci. 26*, 183−189.
(19) Rader, A. J., Anderson, G., Isin, B., Khorana, H. G., Bahar, I., and Klein-Seetharaman, J. (2004) Identification of core amino acids stabilizing rhodopsin. *Proc. Natl. Acad. Sci. U.S.A. 101*, 7246−7251.
(20) Oxenoid, K., and Chou, J. J. (2005) The structure of phospholamban pentamer reveals a channel-like architecture in membranes. *Proc. Natl. Acad. Sci. U.S.A. 102*, 10870−10875.
(21) Schnell, J. R., and Chou, J. J. (2008) Structure and mechanism of the M2 proton channel of influenza A virus. *Nature 451*, 591−595.
(22) Van Horn, W. D., Kim, H. J., Ellis, C. D., Hadziselimovic, A., Sulistijo, E. S., Karra, M. D., Tian, C., Sonnichsen, F. D., and Sanders, C. R. (2009) Solution nuclear magnetic resonance structure of membrane-integral diacylglycerol kinase. *Science 324*, 1726−1729.
(23) Zhou, Y., Cierpicki, T., Jimenez, R. H., Lukasik, S. M., Ellena, J. F., Cafiso, D. S., Kadokura, H., Beckwith, J., and Bushweller, J. H. (2008) NMR solution structure of the integral membrane enzyme DsbB: Functional insights into DsbB-catalyzed disulfide bond formation. *Mol. Cell 31*, 896−908.
(24) Getmanova, E., Patel, A. B., Klein-Seetharaman, J., Loewen, M. C., Reeves, P. J., Friedman, N., Sheves, M., Smith, S. O., and Khorana, H. G. (2004) NMR spectroscopy of phosphorylated wild-type rhodopsin: Mobility of the phosphorylated C-terminus of rhodopsin in the dark and upon light activation. *Biochemistry 43*, 1126−1133.
(25) Klein-Seetharaman, J., Getmanova, E. V., Loewen, M. C., Reeves, P. J., and Khorana, H. G. (1999) NMR spectroscopy in studies of light-induced structural changes in mammalian rhodopsin: Applicability of solution ^{19}F NMR. *Proc. Natl. Acad. Sci. U.S.A. 96*, 13744−13749.
(26) Klein-Seetharaman, J., Reeves, P. J., Loewen, M. C., Getmanova, E. V., Chung, J., Schwalbe, H., Wright, P. E., and Khorana, H. G. (2002) Solution NMR spectroscopy of [α-^{15}N]lysine-labeled rhodopsin: The single peak observed in both conventional and TROSY-type HSQC spectra is ascribed to Lys-339 in the carboxyl-terminal peptide sequence. *Proc. Natl. Acad. Sci. U.S.A. 99*, 3452−3457.
(27) Klein-Seetharaman, J., Yanamala, N. V., Javeed, F., Reeves, P. J., Getmanova, E. V., Loewen, M. C., Schwalbe, H., and Khorana, H. G. (2004) Differential dynamics in the G protein-coupled receptor rhodopsin revealed by solution NMR. *Proc. Natl. Acad. Sci. U.S.A. 101*, 3409−3413.
(28) Loewen, M. C., Klein-Seetharaman, J., Getmanova, E. V., Reeves, P. J., Schwalbe, H., and Khorana, H. G. (2001) Solution ^{19}F nuclear Overhauser effects in structural studies of the cytoplasmic domain of mammalian rhodopsin. *Proc. Natl. Acad. Sci. U.S.A. 98*, 4888−4892.
(29) Werner, K., Lehner, I., Dhiman, H. K., Richter, C., Glaubitz, C., Schwalbe, H., Klein-Seetharaman, J., and Khorana, H. G. (2007) Combined solid state and solution NMR studies of α,ε-^{15}N labeled bovine rhodopsin. *J. Biomol. NMR 37*, 303−312.
(30) Werner, K., Richter, C., Klein-Seetharaman, J., and Schwalbe, H. (2008) Isotope labeling of mammalian GPCRs in HEK293 cells and characterization of the C-terminus of bovine rhodopsin by high resolution liquid NMR spectroscopy. *J. Biomol. NMR 40*, 49−53.
(31) Altenbach, C., Cai, K., Klein-Seetharaman, J., Khorana, H. G., and Hubbell, W. L. (2001) Structure and function in rhodopsin: Mapping light-dependent changes in distance between residue 65 in helix TM1 and residues in the sequence 306−319 at the cytoplasmic end of helix TM7 and in helix H8. *Biochemistry 40*, 15483−15492.
(32) Altenbach, C., Klein-Seetharaman, J., Cai, K., Khorana, H. G., and Hubbell, W. L. (2001) Structure and function in rhodopsin: Mapping light-dependent changes in distance between residue 316 in helix 8 and residues in the sequence 60−75, covering the cytoplasmic end of helices TM1 and TM2 and their connection loop CL1. *Biochemistry 40*, 15493−15500.
(33) Altenbach, C., Klein-Seetharaman, J., Hwa, J., Khorana, H. G., and Hubbell, W. L. (1999) Structural features and light-dependent changes in the sequence 59−75 connecting helices I and II in rhodopsin: A site-directed spin-labeling study. *Biochemistry 38*, 7945−7949.
(34) Cai, K., Klein-Seetharaman, J., Altenbach, C., Hubbell, W. L., and Khorana, H. G. (2001) Probing the dark state tertiary structure in the cytoplasmic domain of rhodopsin: Proximities between amino acids deduced from spontaneous disulfide bond formation between cysteine pairs engineered in cytoplasmic loops 1, 3, and 4. *Biochemistry 40*, 12479−12485.
(35) Cai, K., Klein-Seetharaman, J., Farrens, D., Zhang, C., Altenbach, C., Hubbell, W. L., and Khorana, H. G. (1999) Single-cysteine substitution mutants at amino acid positions 306−321 in rhodopsin, the sequence between the cytoplasmic end of helix VII and the palmitoylation sites: Sulfhydryl reactivity and transducin activation reveal a tertiary structure. *Biochemistry 38*, 7925−7930.
(36) Cai, K., Klein-Seetharaman, J., Hwa, J., Hubbell, W. L., and Khorana, H. G. (1999) Structure and function in rhodopsin: Effects of disulfide cross-links in the cytoplasmic face of rhodopsin on transducin activation and phosphorylation by rhodopsin kinase. *Biochemistry 38*, 12893−12898.
(37) Klein-Seetharaman, J., Hwa, J., Cai, K., Altenbach, C., Hubbell, W. L., and Khorana, H. G. (1999) Single-cysteine substitution mutants at amino acid positions 55−75, the sequence connecting the cytoplasmic ends of helices I and II in rhodopsin: Reactivity of the sulfhydryl groups and their derivatives identifies a tertiary structure that changes upon light-activation. *Biochemistry 38*, 7938−7944.
(38) Klein-Seetharaman, J., Hwa, J., Cai, K., Altenbach, C., Hubbell, W. L., and Khorana, H. G. (2001) Probing the dark state tertiary structure in the cytoplasmic domain of rhodopsin: Proximities between amino acids deduced from spontaneous disulfide bond formation between Cys316 and engineered cysteines in cytoplasmic loop 1. *Biochemistry 40*, 12472−12478.
(39) Resek, J. F., Farahbakhsh, Z. T., Hubbell, W. L., and Khorana, H. G. (1993) Formation of the meta II photointermediate is accompanied by conformational changes in the cytoplasmic surface of rhodopsin. *Biochemistry 32*, 12025−12032.
(40) Sklenar, V., Piotto, M., Leppik, R., and Saudek, V. (1993) Gradient-Tailored Water Suppression for ^{1}H-^{15}N HSQC Experiments Optimized to Retain Full Sensitivity. *J. Magn. Reson., Ser. A 102*, 241−245.
(41) Kumar, S., Sharma, D., Ghosh, G., and Kabir-ud-Din (2005) Structural modifications of aqueous ionic micelles in the presence of denaturants as studied by DLS and viscometry. *Langmuir 21*, 9446−9450.
(42) Kusnetzow, A. K., Altenbach, C., and Hubbell, W. L. (2006) Conformational states and dynamics of rhodopsin in micelles and bilayers. *Biochemistry 45*, 5538−5550.
(43) Tastan, O., Yu, E., Ganapathiraju, M., Aref, A., Rader, A. J., and Klein-Seetharaman, J. (2007) Comparison of stability predictions and simulated unfolding of rhodopsin structures. *Photochem. Photobiol. 83*, 351−363.
(44) Croonen, Y., Gelade, E., Van der Zegel, M., Van der Auweraer, M., Vandendriessche, H., De Schryver, F. C., and Almgren, M. (1983) Influence of salt, detergent concentration, and temperature on the

fluorescence quenching of 1-methylpyrene in sodium dodecyl sulfate with m-dicyanobenzene. *J. Phys. Chem. 87*, 1426−1431.

dx.doi.org/10.1021/bi401557e | *Biochemistry* 2014, 53, 7160−7169